Experiments on the Flow Field and Acoustic Properties of a Mach number 0·75 Turbulent Air Jet at a Low Reynolds Number

Harmen J. Slot · Peter Moore · René Delfos · Bendiks Jan Boersma

Abstract In this paper we present the experimental results of a detailed investigation of the flow and acoustic properties of a turbulent jet with Mach number 0·75 and Reynolds number $3 \cdot 5 \ 10^3$. We describe the methods and experimental procedures followed during the measurements, and subsequently present the flow field and acoustic field. The experiment presented here is designed to provide accurate and reliable data for validation of Direct Numerical Simulations of the same flow. Mean Mach number surveys provide detailed information on the centreline mean Mach number distribution, radial development of the mean Mach number and the evolution of the jet mixing layer thickness both downstream and in the early stages of jet development. Exit conditions are documented by measuring the mean Mach number profile immediately above the nozzle exit. The fluctuating flow field is characterised by means of a hot-wire, which produced radial profiles of axial turbulence at several stations along the jet axis and the development of flow fluctuations through the jet mixing layer. The axial growth rate of the jet instabilities are determined as function of Strouhal number, and the axial development of several spectral components is documented. The directivity of the overall sound pressure level and several spectral components were investigated. The spectral content of the acoustic far field is shown to be compatible with findings of hot-wire experiments in the mixing layer of the jet. In addition, the measured acoustic spectra agree with Tam's large-scale similarity and fine-scale similarity spectra (Tam et al., AIAA Pap 96, 1996).

H. J. Slot (✉) · P. Moore · R. Delfos · B. J. Boersma
Laboratory for Aero and Hydrodynamics, Delft University of Technology,
Leeghwaterstraat 21, 2628 CA Delft, The Netherlands
e-mail: h.j.slot@tudelft.nl

1 Introduction

Inherent to computing limitations, a Direct Numerical Simulation (DNS) of a compressible jet flow is commonly performed on high Mach number jets with a low Reynolds number such as the DNS of Freund [10] and Moore et al. [21]. Before jet flow or jet noise predictions based on a DNS of a turbulent flow can be relied upon, the numerical work need be carefully validated by means of detailed and reliable experimental evidence. The validation would require detailed information of both the flow field and the acoustic far field. There is little experimental data available that would facilitate such a validation of turbulent jets with a high Mach number and low Reynolds number. The documented experimental work on subsonic jets concern measurements focusing either on properties of the flow field or on properties of the acoustic far field. Turbulence characteristics of subsonic turbulent jets with a moderate to high Reynolds number (Re $\approx 10^3 - 10^5$) were reported by Panchapakesan & Lumley [24], Hussein et al. [12], Zaman [40], Wygnanski & Fiedler [38], Laufer and Yen [15] and Bradshaw et al. [7]. Most of the work mentioned concerned low velocity jets (Ma<0·3), and do not or briefly discuss properties of the acoustic far field. Contrary to the aforementioned, Mollo-Christensen et al. [20], Lush [16], Tanna [34] and Ahuja [1] reported properties of the acoustic far field of subsonic turbulent jets in detail, but did not investigate the flow field. Stromberg et al. [29] combined measurements of the acoustic far field and flow field of a subsonic turbulent jet with a low Reynolds number in their work, but used their experimental results mainly to illuminate the process of jet noise production. In addition, little information of the fluctuating flow field was reported. The experimental work reported on in this paper aims to provide accurate and reliable data that can be used for the validation of a Direct Numerical Simulation of a turbulent jet with a Mach number (Ma=U/c) 0·75 and Reynolds number (Re= ρUd/μ) 3.5 ·10^3, where ρ denotes density (kg/m^3), U is the jet flow velocity (m/s), c denotes sound velocity (m/s), nozzle diameter d= 8·10^{-3} (m) and μ denotes dynamic viscosity (Pa·s).

Over the range of Reynolds number considered in a DNS, the effects of Reynolds number have been shown to be important [5, 9]. Study of the jet noise producing mechanisms is relatively less complex with low Reynolds number jets as the range of turbulence scales present in the flow is fairly limited compared to high Reynolds number jets. Consequently, the jet noise producing mechanisms are thought to be more transparent in jets with low Reynolds numbers.

This paper is organised as follows. First, a description of the experimental setup and procedures is given in Section 2. Section 2.1 describes the pressure chamber and the jet exit nozzle in detail. Details concerning the flow field and acoustic measurement techniques and calibration procedures are described in Sections 2.2 and 2.3.

The results are presented in Section 3, and are split into results concerning the flow field (3.1) and the acoustic far field (3.2). Mean flow properties are presented in Section 3.1.1, and concern jet exit conditions, mean Mach number profiles and the development of the jet mixing layer. Fluctuating flow field properties are detailed in Section 3.1.2. The spectral content of density fluctuations in the jet mixing layer are documented, and allow an inspection of the development of the fundamental and the subharmonic mode throughout the jet mixing layer. Spatial linear instability theory is used to asses the axial growth rates as function of Strouhal number.

Table 1 Jet operating conditions	Jet stagnation temperature	T_s	294 K
	Jet massflow	ϕ	$3\cdot1\ 10^{-4}$ kg/s
	Exit centreline velocity	U_j	247 m/s
	Exit centreline Mach number	M_j	0·75
	Reynolds number	Re	$3.5\ 10^3$
	Test chamber pressure	p_c	2170 Pa
	Jet nozzle diameter	D	8·0 mm
	Coordinate system	x, r, θ	
	Strouhal number	fD/U_j	
	Reynolds number	$\rho_j U_j D / \mu_j$	$3.5\ \cdot10^3$

The properties of the acoustic far field are detailed in Section 3.2. The acoustic far field is characterised by overall sound pressure level and spectral content at various angles to the flow direction. A subsequent comparison between the obtained spectral information and Tam's similarity spectra is concluded with a discussion on jet noise generation in subsonic jets.

An overview of the relevant experimental parameters and jet flow conditions is given in Table 1.

2 Description of Experiment

2.1 Pressure chamber and nozzle

For jet flows from a circular nozzle, the peak Strouhal number St=fd/U resides near 0·2. From this, it is clear that acoustic measurements on low Reynolds number jets can be performed at atmospheric conditions but would require a very small jet nozzle diameter (suppose Re=3000, U=300 m/s, $\rho = 1\cdot2$ kg/m^3 then d= 0·15 mm) resulting in extremely high frequencies. To study the flow field for example, there would be a need for expensive optics to perform measurements with a reasonable degree of accuracy and resolution. To circumvent this problem, a semi anechoic pressure chamber has been built in which the pressure can be reduced to a fraction of atmospheric pressure which enables the desired reduction in ambient density. The experimental setup and pressure chamber are depicted in Figs. 1 and 2.

The pressure chamber consists of several segments; one segment is equipped with three circular windows allowing optical access into the chamber. The segments can be interchanged in order to study several stages of jet development or specific features such as jet entrainment (see Figs. 1 and 2).

A circular wooden plate is placed horizontally on a small rim near the bottom of the chamber, onto which a metal foam plate (Recemat, type 2733) is mounted with the purpose to reduce acoustic reflections. The nozzle exit is situated in the centre of the plate, through which the jet proceeds vertically. The jet is thereby effectively issuing from a round orifice in a plate, as depicted in Fig. 1.

The inlet chamber consists of a diffuser with an angle of about 20° followed by a series of five fine irregular mesh screens with an average mesh size of about 1 mm^2 meant to reduce the size of the largest scales present in the flow. A 25:1 contraction is
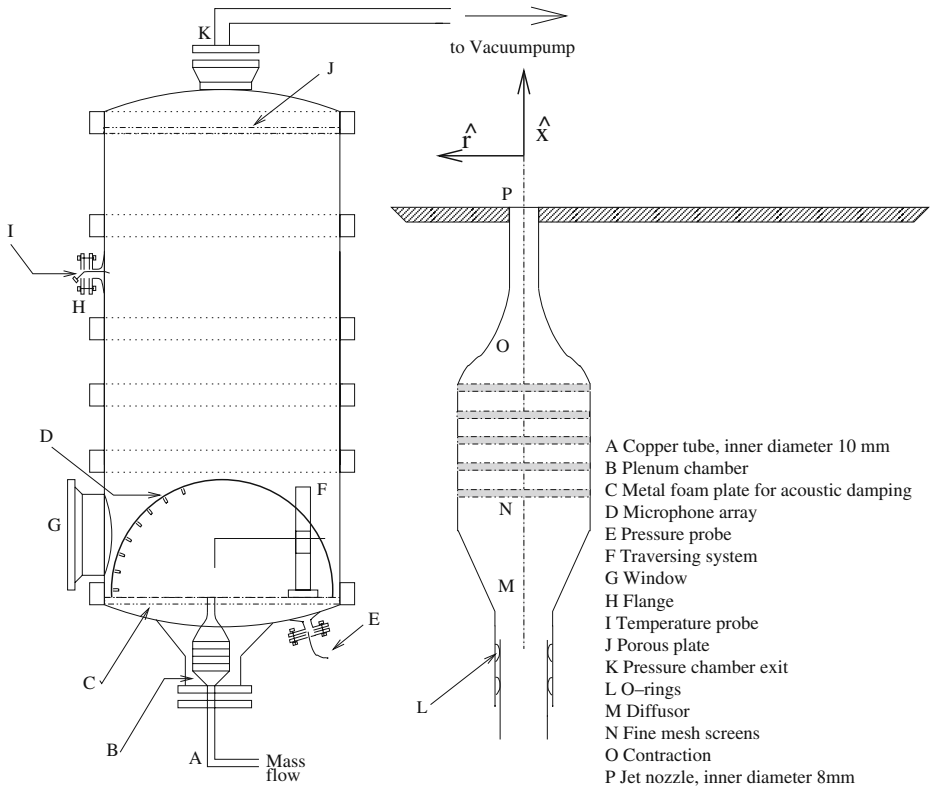
Fig. 1 Schematic of the experimental setup

then followed by a simple 8·0 mm round exit nozzle. The exit nozzle is schematically depicted in Fig. 3. During construction of the nozzle the periphery of the nozzle exit had not been prepared such that it is at right angles with the horizontal. Instead, the edges of the nozzle are slightly chamfered as illustrated in Fig. 3. This causes a sudden but slight expansion of the boundary layer as the flow exits the nozzle.

A well defined mass inflow is ensured by a Bronkhorst HiTec massflow controller type F-202AC-FGA-44-V MFC, capable of delivering a massflow up to 5·0 kg/h. Furthermore, a thermocouple is placed in the stagnation chamber upstream of the contraction to measure the jet stagnation temperature. The temperature inside the pressure chamber is monitored by a second thermocouple, which is injected into the chamber through one of the flanges. A pressure probe is led through a flange near the bottom of the chamber, and read out by a Chell Instruments W60D041111 unheated barocell, with an accuracy of 10 Pa. The pressure inside the tank is brought to a fraction of atmospheric pressure by means of a Rietschle Thomas vacuumpump with a nominal airflow of 250 m³/h, with an end pressure of 10 Pa. To gain better control over variables inside the chamber and to be able to reproduce jets with any combination of Reynolds and Mach number, the vacuumpump must be controllable. To this end, a frequency regulator is connected to the vacuumpump. For the purpose of recording far field jet noise, Sonion 8002 series microphones are mounted on

Fig. 2 Pressure chamber
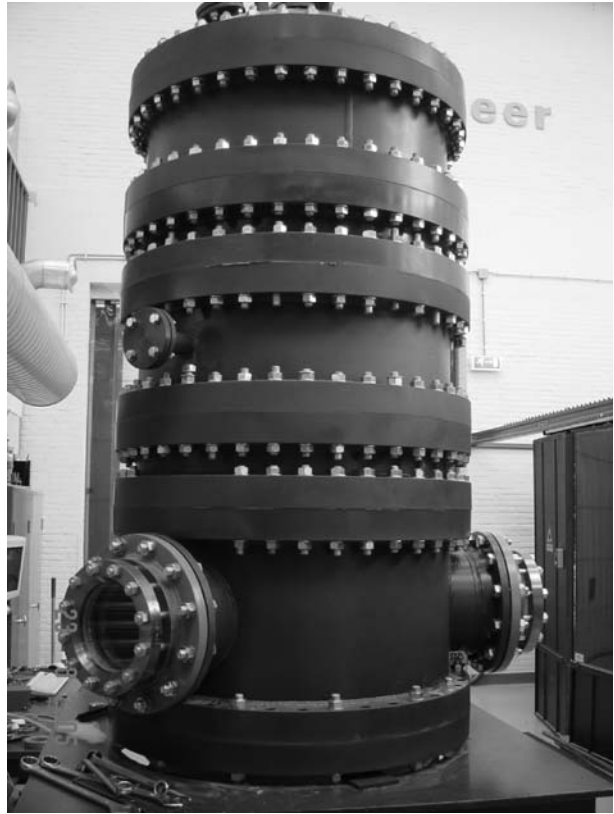
an arc centred above and pointing towards the jet nozzle. The microphones are spaced evenly along the arc (spacing near 5 degrees) and positioned at a distance of 339 mm, equivalent to 42·4 jet diameters from the jet exit. The interior of the pressure chamber and the arc are padded with acoustic damping material. Near the top of the chamber, a porous plate is mounted onto a small rim to ensure a smooth outflow.

Fig. 3 A schematic representation of the exit nozzle (not to scale). The peripheral of the nozzle exit is chamfered, as indicated in the figure
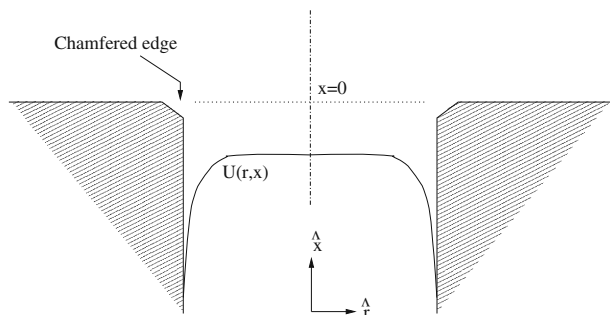
2.2 Flow field measurements

The flow field fluctuations were investigated by means of a hot-wire. The hot-wire data reduction method we follow is a combination of the work of Ko et al. [13] and Morkovin [22]. Ko et al. recognised the potential of their data reduction method by explicitly accounting for the energy transfer to the hot-wire that is returned as end-loss to the hot-wire supports, circumventing the need to define a modified Nusselt number.

After a first series of measurements, the hot-wire bridge voltage fluctuations were found to be approximately proportional to density fluctuations. Normalised fluctuations $T'_{rms}/\overline{T}$ and $u'_{rms}/\overline{u}$ were found to contribute about 5% or less to the output and will not be taken into account here in after. The raw hot-wire signal was filtered by a Butterworth low-pass filter with a cut-off frequency of 25 kHz to eliminate electronic resonances and thereafter sampled at 500 kHz. Details on the followed hot-wire calibration procedure can be found in Appendix A.

A conventional Prandtl tube with an outer diameter of 1·0 mm was used in all mean velocity surveys, except for the measurement of the mean velocity profile immediately downstream of the nozzle exit plane where significant spatial resolution in the jet shear layer is required (Fig. 8a). For this particular investigation the conventional tube was replaced with a glass Prandtl tube with an outer diameter of 100 μm. A differential pressure sensor sensitive up to a pressure difference equivalent to a 140 mm water column was ported to the Prandtl tube and to a second tube, positioned well away from the flow, which measured static pressure. A two dimensional traversing system was used to traverse the Prandtl tube in the spanwise and flow direction.

2.3 Acoustic far field measurements

Acoustic far field measurements are performed using Sonion 8002 series microphones. Assuming that U=300 m/s and St=0·2, we may expect the dominant portion of the noise radiated from a subsonic jet given a 8·0 mm exit nozzle to have frequencies around approximately StU/d ≈ 8 kHz. The microphones are sensitive up to frequencies near 20 kHz, and may therefore be regarded as suitable for performing aeroacoustic measurements on this particular flow. These Sonion microphones are simple electret microphones as shown in Fig. 4. A representative frequency response of the microphone is shown in Fig. 5. The microphones are quite small in size; with their cross sectional diameter of 3·0 mm (≈1/10"), their characteristic dimension is much smaller than the wavelengths of the jet noise propagating to far field. The 8002 series Sonion microphones are not designed to be used for aeroacoustic measurements, and consequently are not calibrated separately by the manufacturer. They come accompanied with specifications that are representative for the entire series. Consequently, each microphone is calibrated separately by means of a pistonphone. For this purpose we use a Grass 240A pistonphone which produces pressure perturbations at a frequency of 250 Hz with a sound pressure level of 113·99 dB at atmospheric conditions. The microphone output signals are read into a computer by two National Instruments PCI 4472 measurements cards. They are equipped with eight input channels and are capable of simultaneously sampling 8 channels at 102 kHz. The specifications further indicate that the input is allowed to

Fig. 4 Schematic representation of the Sonion microphone, with: **a** membrane; **b** backplate and **c** airgap height. All dimensions are in mm
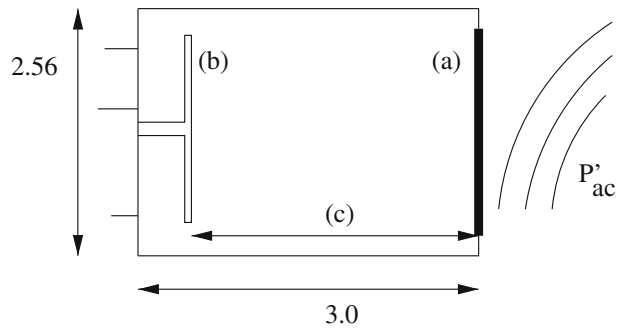
have a maximum peak to peak value of 20 V. To optimise the available resolution on the measurement cards, the output of each microphone is amplified by a specific factor dependent on its output and characteristics. The gain factor is set such that the values sampled by the measurements cards have a peak to peak value of about 14 V, typically.

Some of the properties of the microphone will change with ambient pressure. The relative sensitivity (V/Pa) of the microphone to signals with different frequencies as depicted in Fig. 5 will not change appreciably, i.e. the shape of the sensitivity curve shown in Fig. 5 will not change but the absolute sensitivity will be altered significantly. The microphones are more responsive to pressure perturbations at reduced ambient pressure. The physical background behind this effect is described in detail in Appendix B. For all far field noise measurements in this study, the sampling rate of the PCI measurements card was set at 65536 Hz. Sound pressure level (in dB) data is scaled to atmospheric pressure using the relation

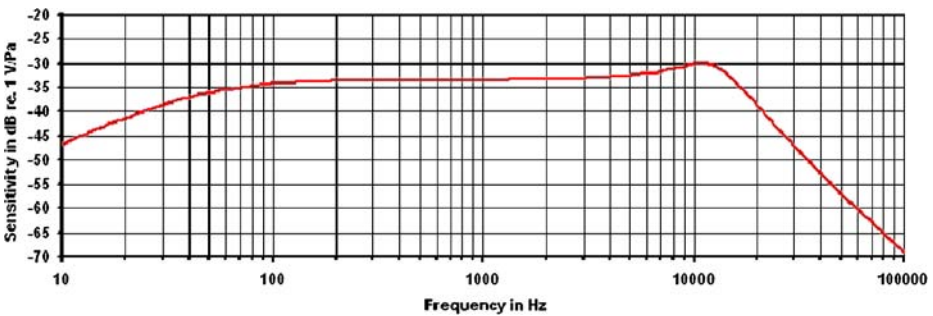$$SPL = 20 \cdot log_{10}\left(\frac{p'_{rms}}{p_c p_{ref}/p_o}\right) \tag{1}$$

Fig. 5 Typical frequency characteristic of a Sonion 8002 series microphone used for far field noise measurements in this study. The sensitivity (V/Pa) is plotted in decibels as function of frequency (Hz)

Where p'_{rms} is the root-mean-square value of the fluctuating sound pressure (Pa), p_o standard atmospheric pressure (Pa), p_c chamber pressure (Pa) and $p_{ref} = 2 \cdot 10^{-5}$ Pa.

To assert the effectiveness of the acoustic damping material, an atmospheric jet noise measurement of a low velocity air jet was carried out in free space and a second with the jet confined within the pressure chamber. The recorded p'_{rms} were scaled up to apply for the low pressure subsonic jet (upon assuming $p'_{rms} \propto U^4$), showing an increase of 1·4 dB in sound pressure level at angles close to the wall when the jet is confined within the pressure chamber in presence of the damping material. This procedure can only give a rough estimate of the error involved, as the recorded noise from the ambient low velocity jet is not of aerodynamic nature and the velocity exponent in assuming $p'_{rms} \propto U^4$ may not be correct. Still, for lack of a better procedure we adopt a 2 dB uncertainty in the sound pressure level due to reverberations.

Furthermore, uncertainty in the determined microphone sensitivity and jet operating conditions add to the uncertainty in the jet noise measurement. The former is asserted by performing an inaccuracy analysis of the relation $p'_{rms} = V^{rms}/(sA)$, where V^{rms} is the rms of the recorded output voltage and A denotes the amplification of the microphone signal. An uncertainty of u(s)= 0·02 V/Pa is a conservative estimate yielding a 0·5 dB uncertainty due to possible microphone calibration errors. The latter concerns uncertainties in the chamber pressure measurement and determination of the jet exit velocity which when combined yield an uncertainty estimated to be 0·5 dB in magnitude. In the obtained sound pressure level data, we therefore assume an overall uncertainty of 3 dB.

3 Results

This section presents results which are believed to be required for reliable validation of a DNS of the same flow. The flow field results in Section 3.1 include information concerning the radial mean Mach number profile in the nozzle exit plane. The effect of the exit nozzle geometry on the flow field development is not trivial, as details of the jet exit conditions may be carried along with the flow as recognised by Boersma et al. [4], Zaman [39] and Bradshaw [6]. Properties of the acoustic far field are presented and discussed in Section 3.2.

3.1 Flow field results

3.1.1 Mean flow field

In Fig. 6 we show the measured centreline mean Mach number distribution.

From Fig. 6, the potential core is estimated to end near x/D=7. This value compares well with values found in literature of potential core lengths of jets with similar jet conditions [21, 29]. The measurements indicate the jet to have a centreline decay constant $B_u = 5\cdot6$ which is in accordance with values found in literature [3, 36]. It is determined from

$$\frac{M_c}{M_j} = \frac{B_u}{x - x_0}. \tag{2}$$

Fig. 6 Axial distribution of mean centreline Mach number
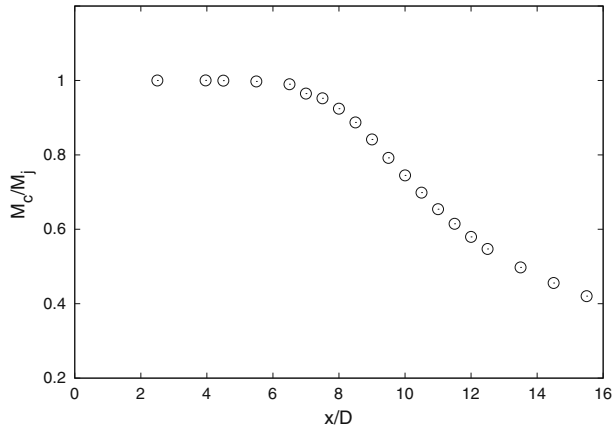
In this equation, M_c denotes the local mean centreline Mach number, x is the axial location normalised by nozzle diameter and x_0 denotes the axial location of the virtual origin, also expressed in nozzle diameter units. A least squares fit with 2 degrees of freedom in parameters B_u and x_0 is applied to the selection of the centreline data at x/D>9·0. Doing so yields $B_u = 5·6$ and $x_0 = 2·6$. To substantiate the claim that the self similar region is reached near x/D=9, the quality of the fit is illustrated in Fig. 7 by plotting $\frac{M_c}{M_j}(x - x_0)$. Indeed, for x/D>9 the decay rate remains constant indicating the self similar region is reached.

Radial mean Mach number profiles are shown in Fig. 8, showing a fairly thick initial mixing layer thickness immediately above the nozzle exit plane. The fairly thick initial mixing layer depicted in Fig. 8 may be thought to be partially due to the finite straight section of tubing prior to the nozzle exit. According to basic fluid

Fig. 7 Decay rate B_u as function of axial position. Plotted is $(M_c/M_j)\cdot(x-x_0)$, and shows B_u to remain constant for x/D>9
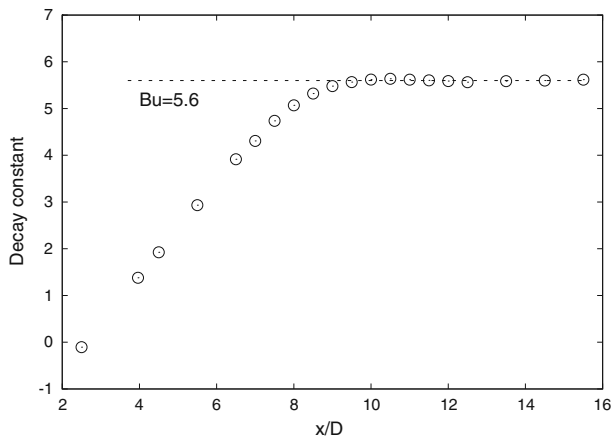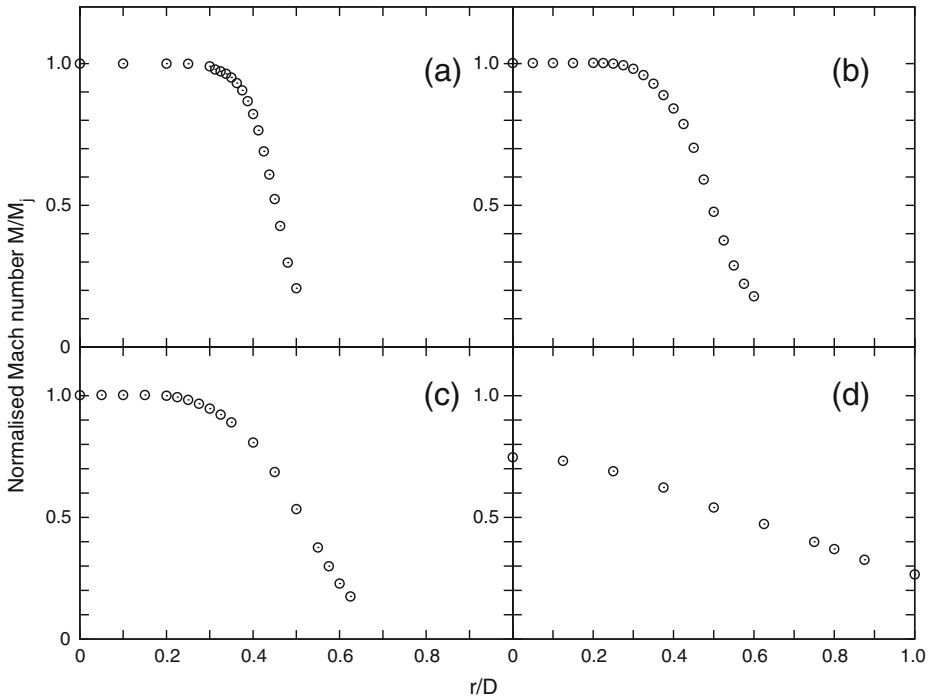
Fig. 8 Radial mean Mach number profile immediately above nozzle exit plane (**a**); and at axial locations x/D: **b** 2·5; **c** 5 and **d** 10

mechanics [2] the thickness of a boundary layer after length x along a horizontal plate may be determined from

$$\delta = \frac{5L}{\sqrt{Re_x}}, \tag{3}$$

in which the Reynolds number is based on length x of the straight section of the nozzle. Based on the above equation, we can estimate the exit mixing layer thickness to be $\delta/2D = 0 \cdot 1$ which is in excellent agreement with the experimentally obtained value of $\delta/2D = 0 \cdot 11$ (see Fig. 11). As mentioned before in Section 2.1, the chamfered edge of the nozzle also contributes to the fairly thick mixing layer at the nozzle exit.

To assert whether the mixing layer immediately above the nozzle exit is laminar, a Blasius profile is superimposed onto the radial mean Mach number data obtained at x/D=0 as depicted in Fig. 9. The figure shows the radial Mach number profile of the initial mixing layer to be in accordance with the Blasius profile, indicating the initial mixing layer is indeed laminar.

A closer examination of the radial mean velocity distributions reveals that all profiles collapse onto a common curve as shown in Fig. 10, in which a curve fit is used similar to the one used by Laufer et al. [14] for subsonic jets. This curve fit takes the form

$$\overline{M}(\eta) = \begin{cases} exp[-2 \cdot 773(\eta + 0 \cdot 5)^2] & \text{for } \eta \geq -0 \cdot 5 \\ 1 & \text{for } \eta \leq -0 \cdot 5 \end{cases}$$

Fig. 9 Confirmation that the mixing layer at x/D=0 is laminar: *circles*, Radial mean Mach number profile; *line*, Blasius profile
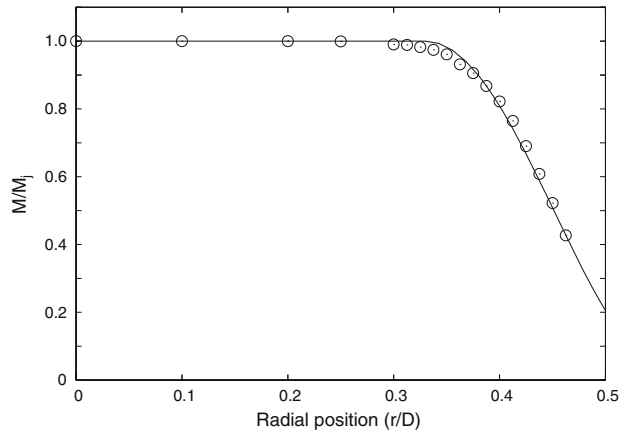
In this equation, the self similarity coordinate $\eta = [r - r(0.5)]/\delta$ in which r(0.5) denotes the radial location at which the local Mach number is exactly 0.5 times the centreline value at that particular axial coordinate.

Let us examine the development of the jet mixing layer more closely. The growth of the jet mixing layer thickness and jet half-radii as fraction of the jet diameter are considered in detail in Fig. 11. Following Troutt & McLaughlin [35], the mixing layer thicknesses δ were calculated from radial mean Mach number profiles upon assuming that $\delta = r(0.1) - r(0.99)$. In Fig. 8 the mixing layer thickness displays a moderate growth in the early development stages, as shown in Fig. 11. Shortly before the end of the potential core is reached, the mixing layer thickness displays a rapid radial expansion. We may therefore conclude that transition from a laminar to a turbulent mixing layer occurs between 5 to 6 jet diameters downstream, after which the growth rate of the mixing layer thickness is significantly increased. After the end of the potential core, the mixing layer thickness grows approximately linear with axial distance.

Fig. 10 Radial mean Mach number profiles plotted against self similarity coordinate η at axial locations x/D: *circles*, 2.5; *upsidedown triangles*, 5; *right-side-up triangles*, 10
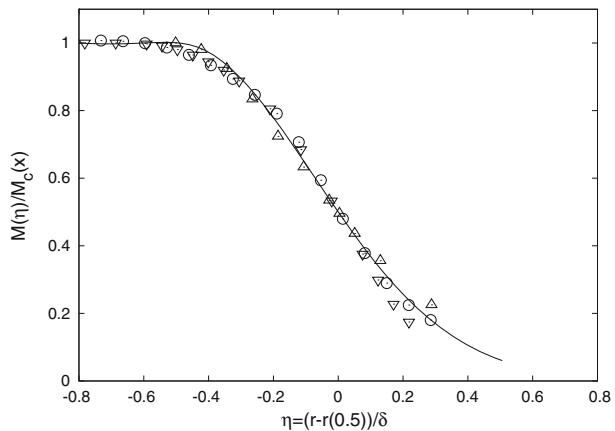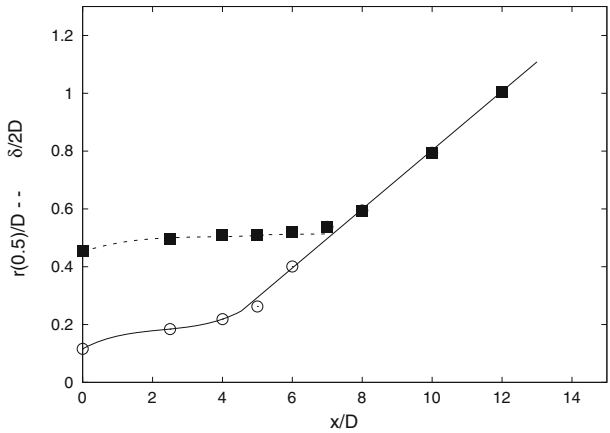
Fig. 11 Jet mixing layer
development, characterised by
mixing layer thickness $\delta/2D$:
circles and jet half radii
r(0·5)/D: *squares*

3.1.2 Fluctuating flow field

Density fluctuations as fraction of local density are shown in Fig. 12. During the first couple of jet diameters downstream of the nozzle exit the density fluctuations grow approximately exponentially with distance within the jet mixing layer, as fraction of the local density. The density fluctuations as fraction of local mean density saturate in amplitude near x/D= 3·5, and remain in the same order of magnitude until x/D=6 after which a gradual decay is set in. The decay is most likely linked with the effects of jet spreading, which becomes significant once the potential core has collapsed near x/D=7.

The density fluctuations in the mixing layer find significant contributions from fluctuations with specific frequencies, as illustrated in the hot-wire spectra shown in Fig. 13. The hot-wire spectra are based on 16384 point Fourier transforms on 400 windows yielding an averaged spectrum with a 30·5 Hz spectral resolution. From the figure it becomes apparent that the fluctuations in the jet mixing layer are initially dominated by instabilities centred around a relatively discrete frequency

Fig. 12 Density fluctuations
as fraction of local mean
density at several probe
locations in the shear layer.
Data was gathered at the
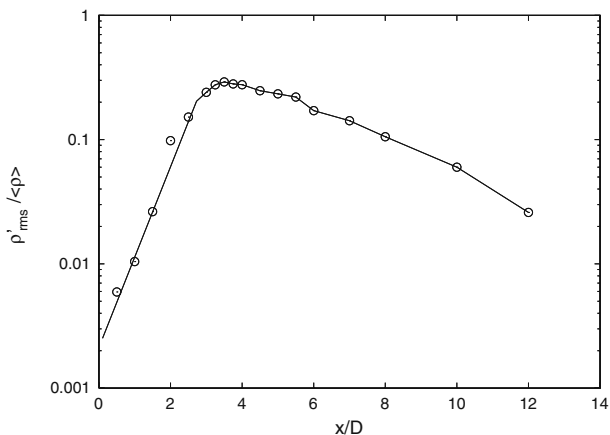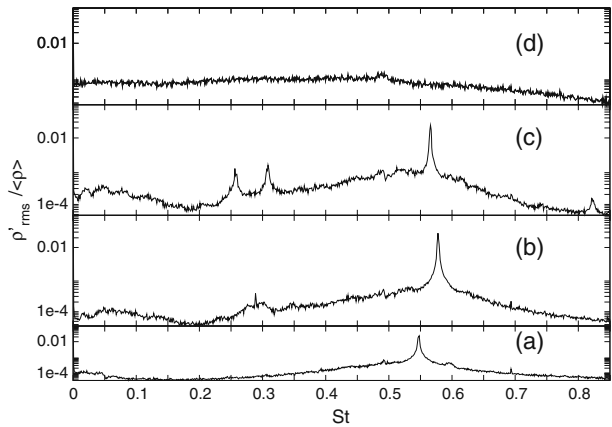radial location of maximum
fluctuation level

Fig. 13 Spectral content of hot-wire signal recorded in the mixing layer at locations x/D: **a** 3; **b** 4·; **c** 5 and **d** 10. Data obtained at radial positions of maximum fluctuation level

near Strouhal number St= 0·54, which corresponds to the fundamental Strouhal number based on jet diameter and centreline exit velocity. These instabilities are seen to dominate the spectra during the first few diameters downstream from the nozzle exit. Its subharmonic near St= 0·27 formed by vortex pairing is identified in Fig. 13b. In the self-similar region at x/D=10 the spectrum is seen to be classically broadband.

The development of the fundamental mode and its subharmonic is illustrated in Fig. 14. Initially, the fundamental mode near St= 0·54 grows approximately exponential with distance in accordance with laminar instability theory [18]. Its subharmonic is two order of magnitudes smaller when the fundamental mode saturates in amplitude. Once the fundamental mode has saturated in amplitude, a similar (but slightly less rapid) exponential growth of the subharmonic mode is observed between x/D= 3 − 4·5, after which the subharmonic mode saturates in amplitude and a gradual decay is set in. The decay is seen to be set in near x/D=7, which coincides with the location of the end of the potential core. Therefore it is likely that the decay

Fig. 14 Development of spectral components St= 0·55 and St= 0·27 through the jet mixing layer: *squares*, St= 0·54; *circles* St= 0·27; *circles on the line* total signal. Data points are maxima within band-passed spectra, gathered at locations of maximum fluctuation level
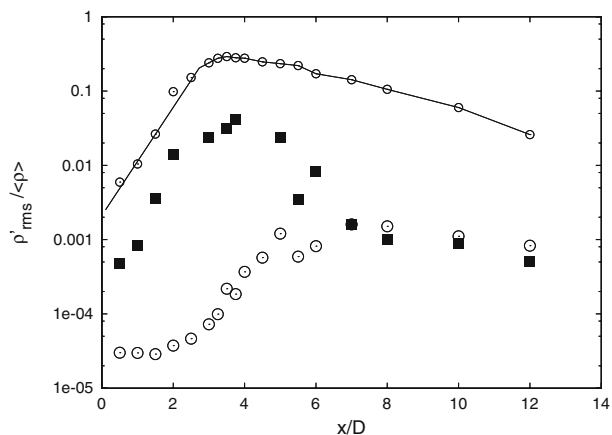
in density fluctuations are connected to the spreading of energy over a larger radial distance within the jet.

Figure 15 shows radial profiles of density fluctuations in the jet mixing layer as fraction of local mean density. It shows that as one progresses downstream from the nozzle through the jet high density fluctuation level shift towards the jet centreline, in accordance with the narrowing of the potential core and flattening of mean velocity profiles. By x/D=5, the peak has nearly reached the centreline indicating the mixing layer is rapidly spanning the entire width of the jet.

As is well known and illustrated in Fig. 14, fluctuations at lower Strouhal numbers develop more gradually closer to the nozzle exit than fluctuations at high Strouhal numbers [8]. The rapid growth in amplitude of the fundamental mode near St= 0·54 suggests that it may be the most instable mode in this jet. This may be further investigated by noting that in spatial instability theory any fluctuating property can be represented mathematically as [17, 33]

$$p(x, r, \theta, t) = A(r)e^{-k_i x + i(k_r x + n\theta - \omega t)}. \qquad (4)$$

In this equation, k_i denotes the axial growth rate of an instability with a pure real frequency ω. To examine the axial growth rate of the density fluctuations, data need to be taken at constant radial distance. Small deviations may occur in the spectral location of an instability, as the subharmonic mode for example may be observed near St= 0·27 as well as near St= 0·25, which is likely to be connected to local velocity variations within the jet mixing layer. As a consequence, the spectral information is band-passed such that the peak amplitude of an instability at a certain axial location is sought within band-passed spectra defined by $St_a = St_c \pm 0·02$ where St_c is the centre frequency of the band-passed interval (this bandwidth is chosen fairly arbitrarily, but is wide enough such that the obtained peak amplitude within that interval is at the same frequency as over a significantly wider interval). An exponential model is fitted to the obtained fluctuation maxima for all axial locations that lie within the region of exponential growth by means of a least squares fit. The slope of the fit corresponds to the axial growth rate of the band-passed frequency, for which the results are shown in Fig. 16.

Fig. 15 Radial distribution of density fluctuations as fraction of local mean density at several axial probe locations x/D: **a** 1; **b** 3; **c** 5; **d** 7 and **e** 10
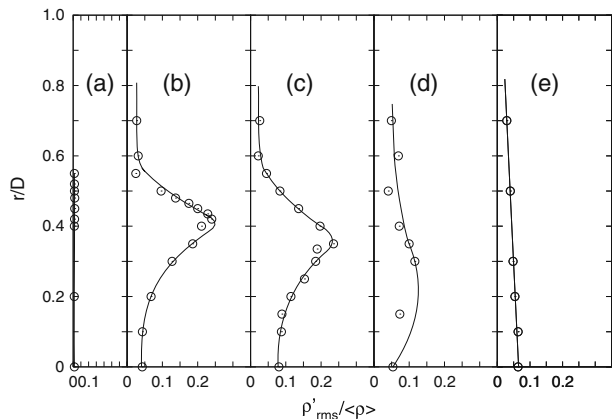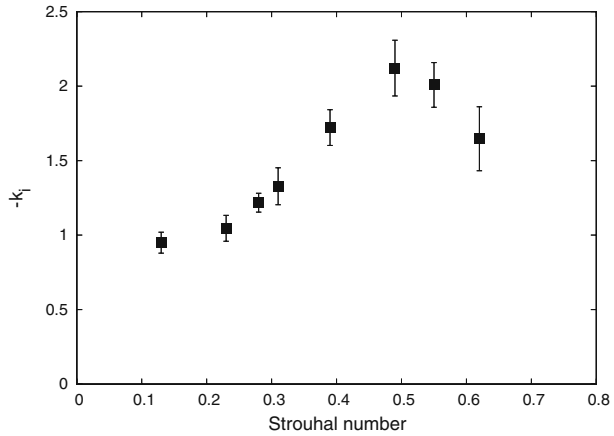
Fig. 16 Fluctuation growth rate as function of frequency. The growth rates are calculated with data obtained in regions of exponential growth. All data taken along the line r=D/2


The axial growth rate displays a slow increase at low frequencies, after which an approximate linear relationship with Strouhal number is observed for $0.3 \leq St \leq 0.5$. The most unstable mode is seen to reside near $St = 0.5$, which confirms to the observed behaviour of frequencies near $St = 0.54$ shown in Fig. 13a. The dependence of the Strouhal number of the most unstable mode does not strongly depend on the initial momentum thickness of the shear layer [19]. At low Strouhal numbers, the deviation from the linear trend observed at intermediate Strouhal numbers $0.3 < St < 0.5$ may be attributed to combination of a change in governing length scale from the local vorticity thickness to nozzle diameter and effects of jet spreading. As the axial wavelength of instabilities become longer at low frequencies, the governing length scale over which growth is exhibited is determined by the nozzle diameter. At axial distances comparable to a few nozzle diameters, it is probable that the mechanism by which the instabilities grow is weakened by the effect of jet spreading. This effect is avoided by instabilities with short axial wavelengths, i.e. by instabilities of which the development is governed by the local vorticity thickness. Axial growth rates of instabilities with Strouhal numbers above $St = 0.7$ are not included in the figure, as no significant length of exponential growth could be found in the data. Note that the error bars are due to uncertainties inherent from the linear fit.

The growth of the fundamental mode dominates the hydrodynamic behaviour of the flow during the first few diameters downstream of the nozzle exit. Beyond $x/D = 3.5$, the fundamental mode has saturated in amplitude and gradually decays downstream. The growth of the fundamental mode manifests itself in a pronounced manner, visible by the formation of large coherent structures during the stages of initial growth of the jet. The axial development of coherent structures may be investigated by autocorrelating the hot-wire data. The integral timescale is defined as

$$T(x) = \int_0^{T*} R(x, \tau) d\tau. \tag{5}$$

Generally, the autocorrelation function shows to exhibit some negative loops which complicates an accurate computation of the integral time scale. Truncating the autocorrelation function at time $T*$ at which $R(x, \tau)$ has its first zero passage has

Fig. 17 Integral time scales: *circles* at radial locations of maximum fluctuation level; *squares* along the line r=D/2
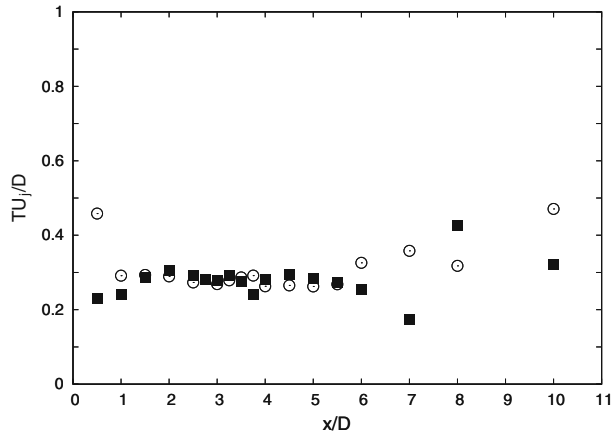
shown to be an effective method to deduce an accurate integral timescale from the hot-wire signal [23, 27, 30].

In an Eulerian frame of reference, the hot-wire data only gives information on the spatial structure of the flow and not so much on the timescales of the turbulence itself. Figure 17 shows the normalised integral timescale T along the line r=D/2 and along the line of maximum fluctuation level. The integral timescale has been nondimensionalised as TU_j/D in which U_j is the jet centreline exit velocity and D is jet nozzle diameter.

From Fig. 17 we may conclude that the spatial extend of the coherent structures increases shortly downstream of the nozzle exit, and remains fairly constant between approximately x/D= $2 \cdot 5 - 4.5$. As the mixing layer becomes turbulent between x/D= $5 - 6$, a sudden drop in integral time scale is observed along r=D/2. The spatial extend of the coherence in density fluctuations is thus severely reduced in regions in the vicinity of the jet periphery, which may be attributed to the dissipative nature of the turbulent mixing layer. Flow structures with significant spatial coherence may still be registered in the vicinity of the centreline of the jet for x/D>5, as radial locations of maximum density fluctuation level were observed to shift towards the centreline for x/D>5 as shown in Fig. 15. An increase in integral time scale is observed near r=D/2 once the potential core has collapsed.

3.2 Acoustic far field results

Sound pressure level (SPL) directivity is shown in Fig. 18. The directivity pattern displays a maximum near 30° to the flow direction, in agreement with previously reported directivity patterns of subsonic jets [16, 20, 29, 34]. No information at angles smaller than 18·5° is shown, as the acoustic data in this region would be contaminated by hydrodynamic pressure fluctuations.

The spectral content of the acoustic signal recorded at various angles to the flow direction is shown in Fig. 19. The spectra are based on 1024 point Fourier transforms on 840 windows yielding an averaged spectrum with a 64 Hz spectral resolution. Near the angle of maximum noise emission, the spectrum of the acoustic signal is quite directional in nature and has a maximum contribution from pressure fluctuations

**Fig. 18** Overall sound pressure level data at 30 jet diameters from nozzle exit
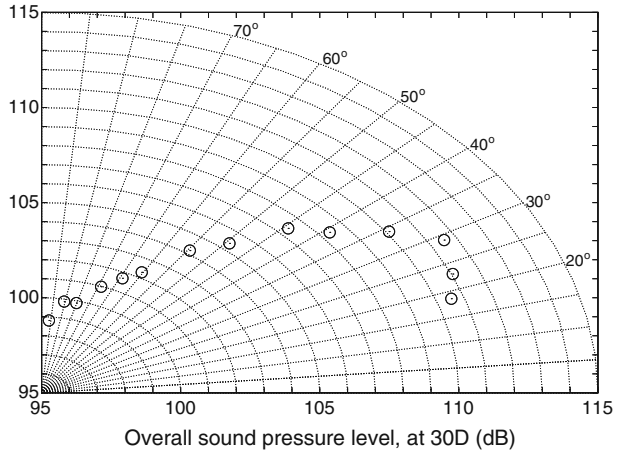
centred around St= 0·27. This indicates that the axisymmetric subharmonic mode is the most effective noise generator in this jet.

The observed behaviour of the spectra to shift from a frequency dependent to a more uniform nature with increasing angle is well-known. The physical background for the observed change in spectral shape is not universally agreed upon. Classically, the enhanced forward radiation efficiency of low frequencies is thought to be due to source convection. In this framework of thought, the sound sources are thought to move with the mean flow. It is not that difficult to verify that moving sources will radiate more noise in their propagation direction. Similarly, the relatively low sound pressure level of high frequencies at angles close to the flow direction is classically recognised to be mainly due to sound refraction by the mean flow.

Evidence of vortex pairing in the mixing layer is presented in Fig. 13. Vortex pairing may indeed be expected to occur in subsonic jets in the mixing layer, and are known to be efficient noise generating mechanisms [11, 28, 29]. The Strouhal number of the peak value of the overall sound pressure level at angles close to the

Fig. 19 Spectral content of far field noise at several angles to the flow direction: **a** 18°; **b** 34° and **c** 49°
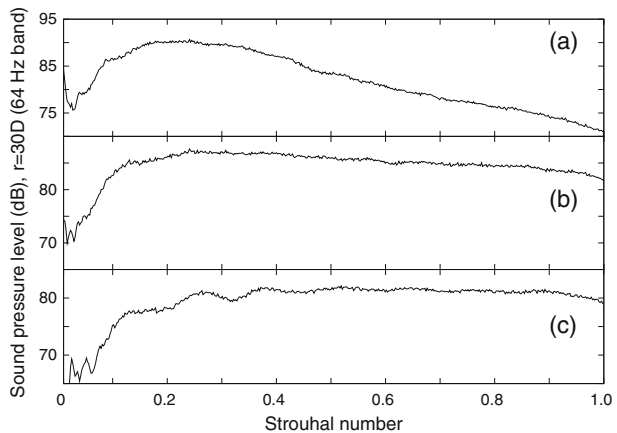
flow direction resides near the Strouhal number of the subharmonic mode, indicating that it is likely that the process of vortex pairing in the mixing layer contributes significantly to the amplitude of the overall radiated acoustic far field.

Recently, the noise spectra of high-speed jets were shown to exhibit self-similarity by Tam et al. [32]. Similar to subsonic jets, the noise spectra of high-speed jets at large angles to the flow direction are quite uniform in nature and are believed to be caused by the fine-scale turbulence in the flow. This type of sound is well described by Tam's fine-scale similarity spectrum (FSS). In high-speed jets, large turbulence structures/instability waves are efficient noise generators and radiate sound in a highly directional fashion. Instability waves moving at supersonic velocity relative to the ambient medium generate Mach wave radiation. This mechanism is very effective in high-speed jets, and radiates sound waves in directions close to the jet flow direction. The spectra close to the jet flow direction were found to be well described by Tam's large-scale similarity spectrum (LSS). It was argued that the observed dual nature of jet mixing noise of supersonic jets also applies to subsonic jets, as the convective Mach number was found to be a proper governing parameter of jet mixing noise.

If the data confirms to previous evidence [32, 37] in which the above suggestion found support, then the measured spectra of the current subsonic jet should fit Tam's FSS and LSS.

This is examined by comparing the measured spectra to the LSS and FSS spectra of Tam as shown in Fig. 20. In the figure, the peaks of the similarity spectra are positioned to overlap the peaks of the measured spectra. Indeed, at 23° to the flow direction the measured spectrum matches the LSS spectrum accurately for frequencies up to 20 kHz, after which the signal starts to deviate significantly from the LSS. Considering the frequency response of the Sonion microphone as depicted in Fig. 5, we may attribute the mismatch to a drop in response of the microphone for frequencies above 20 kHz. In contrast, at 34° to the flow direction the recorded low frequent pressure fluctuations confirm to the LSS spectrum but an increase in amplitude in the high-end of the spectrum causes an offset between the LSS and the measured spectrum. The FSS spectrum is included in the figure to indicate the measured spectrum appears to contain a combination of both.

Near 64° from the flow direction, the shape of the measured spectrum confirms reasonably to the FSS spectrum. The low-end and high-end of the spectrum does not match the FSS spectrum. Similar to previous observations, the deviations for frequencies above 20 kHz observed in the figure are likely due to a drop in microphone sensitivity to these frequencies. In comparing Figs. 20c and 20d, the discrepancy at lower frequencies between the measured spectrum and the FSS spectrum has increased with angle. This effect may be explained by noting that the distance between the microphone and the metal foam plate decreases with increasing angle to the flow direction, and might become comparable to the wavelength of acoustic waves with a low frequency. The microphone at 86° to the flow direction is mounted approximately 2·3 cm above the metal foam plate. Given the ambient sound velocity $c_\infty \approx 344$ m/s and the threshold wavelength of 2·3 cm, we obtain $f \approx 14\cdot8$ kHz. Similarly, the microphone at 64° is mounted approximately 14·7 cm above the horizontal, resulting in a threshold absorption frequency near 2·3 kHz. We therefore consider it plausible that acoustic waves with wavelengths comparable to $\lambda = 2 \cdot 3$ cm or less are partially absorbed by the metal foam plate resulting in the
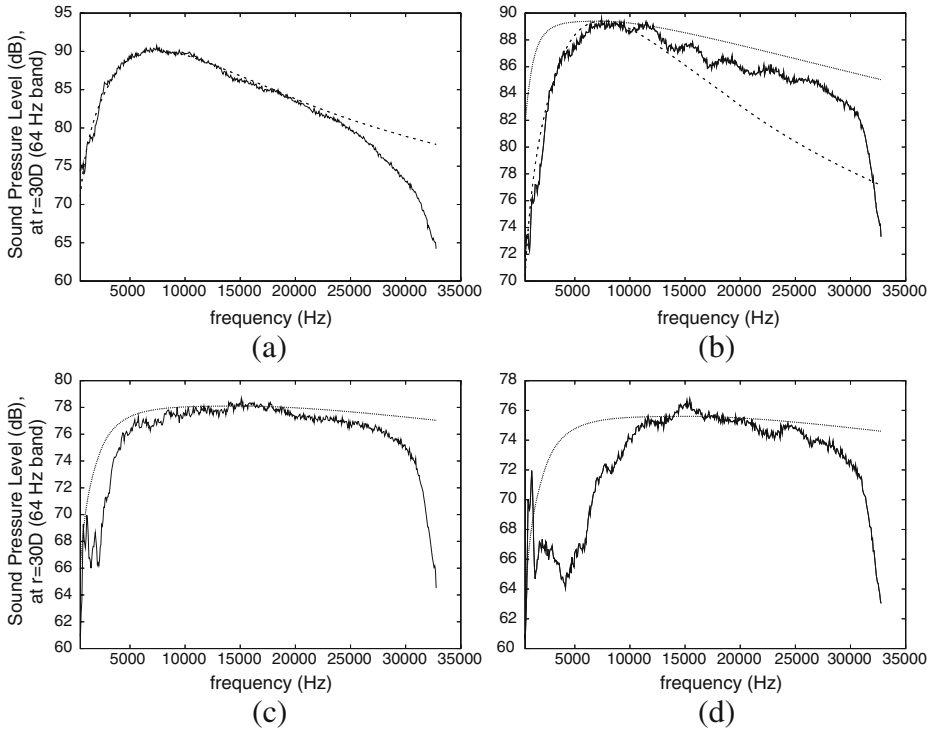
Fig. 20 Measured spectra are compared against the similarity curves of Tam. Shown are measured spectra obtained at: **a** 23° and LSS (*dashed*); **b** 29° compared to both LSS (*dashed*) and FSS (*finely dashed*); **c** 64° and FSS (*finely dashed*); **d** 86° and FSS (*finely dashed*)

corrupted low-end of the spectrum observed in Fig. 20d. This particular wavelength corresponds to a frequency near 14·8 kHz which is indeed near the frequency below which the spectrum in Fig. 20d is seen to deviate significantly from the similarity spectrum. The absorption threshold frequency estimate of 2·3 kHz at 64° is also in reasonable agreement with the frequency below which the measured spectrum deviates from the FSS, reinforcing the belief that the metal porous plate effects the low-end of the measured spectra at large angles to the flow direction.

Furthermore, oscillations are visible in the middle segment of the spectrum obtained at 86° which are not as significant at smaller angles to the flow direction. The oscillations that are visible in the same figure are reminiscent of interference patterns, and may therefore be attributed to interference of partially reflected acoustic waves from the chamber wall and incident acoustic waves.

Additional insight is gained into the directivity of spectral components by considering Fig. 21, in which the sound pressure level of a selection of spectral components are shown as function of angle to the flow direction.

The directivity of the St= 0·27 component shows to have an increased radiation intensity in the 20° direction, distinctly different in comparison to the directivity of other spectral components observed in the mixing layer instabilities shown in Fig. 13. The sound pressure level of the St= 0·27 component reaches its maximum

Fig. 21 Sound pressure levels of main acoustic spectral components recorded in the far field. Components correspond to peak amplitudes found in hot-wire spectra: *squares*, St= 0·27; *circles*, St= 0·54
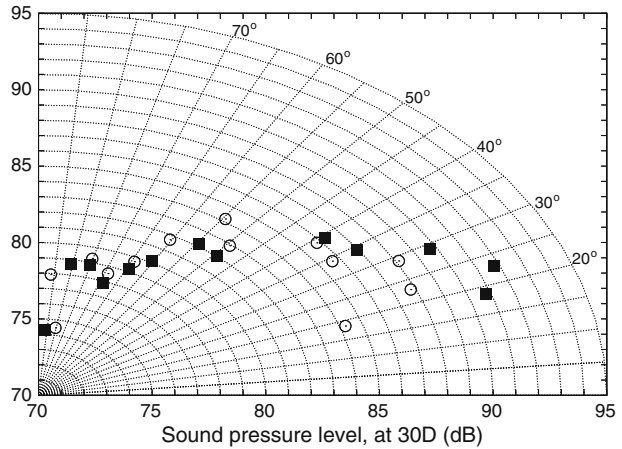
at smaller angles to the flow direction than the angle at which the overall maximum sound pressure level is observed, which is indeed near 30° to the flow direction. The fact that the radiation direction of the St= 0·27 component reaches its maximum at smaller angles to the flow direction than other components, agrees with the radiation characteristics of large turbulence structures/instability waves in high-speed jets.

As the measured spectra at angles close to flow direction fit Tam's large-scale similarity spectra, we may conclude that the observed high noise intensity inside the cone of silence is due to acoustic radiation with characteristics similar to Mach wave radiation. Mach wave radiation is generally not recognised to occur in subsonic jets, as the convective Mach number is too low to yield a substantial portion of the wavenumber spectrum that has supersonic phase velocity.

Tam & Burton [31], Tam et al. [32] and later on Viswanathan [37] proposed a mechanism by which an acoustic wave may be radiated in a subsonic jet with features similar to Mach wave radiation. The proposed mechanism involves recognising the importance of amplitude modulation of instability waves. An instability wave moving at subsonic velocity and constant amplitude cannot generate Mach wave radiation, as none of its spectral components has supersonic phase velocity; its spectrum is discrete. An instability wave which is allowed to change its amplitude does not have a discrete spectrum, but a spectrum that is broadband. Realizing that if the instability wave has a rapid growth and subsequent destruction its spectrum could have spectral components with supersonic phase velocity, then the average phase velocity of the wave packet comprising the instability wave need not be supersonic. This mechanism merely requires a rapid growth and destruction of instability waves such that the spectrum does have components with supersonic phase velocity.

Such a violent growth and destruction of instability waves in subsonic jets may be found applicable to instability waves at low Strouhal numbers, which develop more gradually closer to the nozzle exit and begin their exponential growth further downstream and attain their peak amplitude close to the end of the potential core. If the process sketched above is rigorous enough, it seems plausible that this mechanism may generate the acoustic radiation with characteristics similar to Mach wave radiation observed in this subsonic jet.

In the hydrodynamic regime in which the hot-wire measurements were taken, the density fluctuations may have contributions from linear and non-linear disturbances. Outside regions of exponential growth, we cannot therefore solely associate the data with instability waves and provide direct evidence of such rapid destruction. Recent measurements of Panda & Seasholtz [25] provide some interesting trends that support the aforementioned mechanism. They investigated the axial variation of density fluctuations along the jet centreline and along the jet peripheral mixing layer. Pressure fluctuations at low Strouhal numbers recorded with a microphone located close to the jet flow direction showed significant correlation with density fluctuations just downstream of the end of the potential core for jets with both subsonic and supersonic Mach numbers. This shows that the region close to the end of the potential core to be a low-frequency sound source for both subsonic and supersonic jets, and reinforces the notion that acoustic waves with features similar to Mach waves can be generated in subsonic jets by amplitude modulation of instability waves.

4 Concluding Remarks

The data in this paper is considered to be suited for the validation of a Direct Numerical Simulation. Apart from the axial mean velocity distribution, we have presented detailed information concerning the radial velocity profiles and mixing layer thicknesses in the early stages of jet development. Such information is critical in order to understand the manner in which the jet develops, and even more so if predictions made by a DNS are to be compared with experimental data obtained in downstream regions or in the far field.

Additionally, properties of the fluctuating flow field in terms of hot-wire spectra and density fluctuations were presented. The turbulence information provided in this paper is limited to characteristics of the density fluctuations, as the hot-wire is quite insensitive to velocity and temperature fluctuations when the ambient pressures is drastically reduced. The fluctuating flow field was characterised by the axial development of density fluctuations along the mixing layer and by documenting their radial development at several stations along the x-axis. The fundamental mode is the most unstable mode in this jet, as became apparent by calculating the growth rates of density fluctuations in regions of exponential growth.

The subsequent formation of its subharmonic is most interesting, as it may be expected that vortex pairing in the jet mixing layer is an efficient noise generating mechanism in subsonic jets. The acoustic spectra of the radiated far field show that pressure fluctuations with frequencies near that of the subharmonic mode are the most effective noise generators in this jet.

In addition, the acoustic spectra at angles close to the flow direction were shown to be well described by Tam's large-scale similarity spectrum, and has features reminiscent to that of Mach wave radiation. The evidence presented in Section 3.2 indicate that subsonic jets may generate acoustic waves with characteristics similar to those of Mach wave radiation.

Appendix A: Hot-Wire Calibration Method

Following Perry [26], the fluctuation e' of the bridge voltage caused by a hot-wire ran in Constant Temperature Anemometry (CTA) mode can be written in the following form

$$\frac{e'}{\overline{E}} = A_u \frac{u'}{\overline{u}} + A_\rho \frac{\rho'}{\overline{\rho}} - A_T \frac{T_o'}{\overline{T_o}}. \tag{6}$$

The coefficients A_i mentioned above can be interpreted as velocity, density and temperature sensitivity coefficients, respectively. To relate the hot-wire bridge voltage output to specific flow properties at the hot-wire probe location, the sensitivity coefficients need be determined by means of calibration. Determining their individual values involves evaluating various logarithmic derivatives of parameters describing the local heat transfer from the hot-wire to the surrounding fluid. The exact form of the expressions A_i are mentioned in [22], and will not be repeated here.

Any sensitivity coefficient can in principle be determined by placing the hot-wire in the laminar region of the jet and relating the hot-wire bridge output to a series of known flow conditions, with the restriction that the other variables remain constant during the series of flow conditions. It may be expected that the hot-wire is most responsive to density changes [29], thus we shall calibrate A_ρ and deduce the values of the two remaining sensitivity coefficients from knowledge of A_ρ. For a given hot-wire overheat ($\tau_{wr} = (R_{hot} - R_{cold})/R_{cold}$), the value of A_ρ can be derived from the hot-wire bridge output as function of the mean jet core density at constant jet exit velocity and jet stagnation temperature. More specifically,

$$A_\rho = \frac{\partial ln\overline{E}}{\partial ln\overline{\rho}}\bigg|_{T_o,u}. \tag{7}$$

A typical graph from which A_ρ can be determined is shown in Fig. 22. For a given hot-wire overheat, the output voltage is monitored as function of mean jet core density. This process is repeated for several hot-wire overheats. The value of A_ρ at a certain hot-wire overheat may now be determined from a least-squares fit of relation (7) to the data and setting A_ρ equal to its slope.

Fig. 22 Typical hot-wire calibration curves from which A_ρ may be deduced. In the figure, the output voltage is plotted as function of the mean jet core density on a double logarithmic scale. According to Eq. 7, values of A_ρ can be determined from a linear fit of the data obtained with a given hot-wire overheat
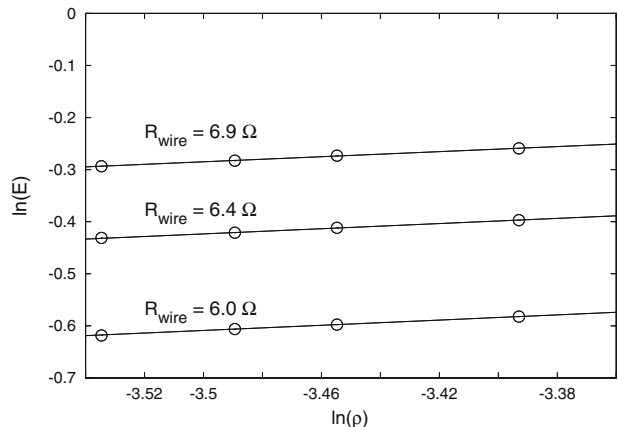
All other parameters may be calculated from knowledge of A_ρ. After a first series of measurements, the hot-wire bridge voltage fluctuations were found to be approximately proportional to density fluctuations. Normalised fluctuations $T'_{rms}/\overline{T}$ and $u'_{rms}/\overline{u}$ were found to contribute about 5% or less to the output and are not taken into account.

## Appendix B: Microphone Behaviour at Reduced Ambient Pressures

A model describing the sensitivity (V/Pa) of the Sonion microphones is based on parameters such as the acoustic impedance due to squeeze damping, membrane stiffness and airgap volume. To understand the behaviour of the microphones at reduced ambient pressures, it is vital to recognise that the acoustic compliance of the airgap is linearly related to the ambient pressure

$$C_{vol} = \frac{hS}{\gamma p_o} \qquad [m^3/Pa]. \tag{8}$$

In this equation, h denotes the height (m) of the airgap between the membrane and backplate, S is a representative value for the cross sectional area (m^2) of the airgap, p_o denotes the ambient pressure (Pa) and specific heat ratio $\gamma = 1 \cdot 4$. The volume of air contained within the microphone will become more responsive to pressure fluctuations as the ambient pressure is reduced. Beyond a certain threshold the acoustic compliance of the microphone system will be limited by the characteristics of the membrane and further reduction of the ambient pressure has no net effect on the sensitivity of the microphone. This effect is confirmed by examining the sensitivity as function of ambient pressure, of which the results are shown in Fig. 23. The threshold below which the sensitivity of the microphone can be regarded constant is seen to reside near 8000 Pa.

All measurements reported on in this paper were conducted well below this threshold value. Apart from the sensitivity of the microphone, the effect of a reduction of ambient pressure onto the RMS value of the pressure perturbations generated by the pistonphone during calibration need be asserted. To this end,

Fig. 23 Sensitivity curve of a microphone as function of ambient pressure. Individual sensitivity curves may differ from one microphone to the other due to difference in material properties
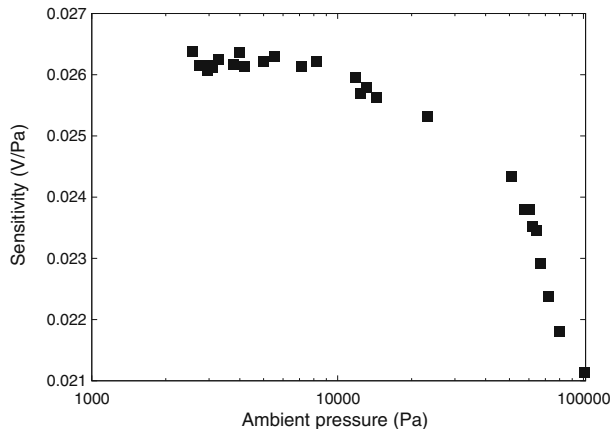
consider a piston moving frictionless inside a cylinder. The process is adiabatic, and therefore the differential relationship between p and V follows

$$dp = -\gamma p \frac{dV}{V} \rightarrow p' \propto p_o.$$

This implies there is a linear relationship between ambient pressure and the acoustic output of the pistonphone. Consequently, the p'_{rms} input to the microphone during calibration can be easily calculated from its known value at standard atmospheric conditions;

$$p'_{rms} = \left(\frac{p_c p_{ref}}{p_0} \right) \cdot 10^{SPL_0/20}.$$

In this relation, SPL_0 denotes the sound pressure level of the pressure perturbations generated by the pistonphone at atmospheric conditions as specified by the manufacturer and equals $SPL_0 = 113 \cdot 99$ dB. Furthermore, p_c represents the chamber pressure (Pa), p_0 is standard atmospheric pressure (Pa) and $p_{ref} = 2 \cdot 10^{-5}$ (Pa).

References

1. Ahuja, K.K., Bushell, K.W.: An experimental study of subsonic jet noise and comparison with theory. J. Sound Vib. **30**, 317–341 (1973)
2. Batchelor, G.K.: An Introduction to Fluid Dynamics. Cambridge University Press, Cambridge (1967)
3. Bodony, D.J., Lele, S.K.: Jet noise prediction of cold and hot subsonic jets using large-eddy simulation. In: Conference paper presented at the 2004 AIAA conference, AIAA Pap. 2004–3022 (2004)
4. Boersma, B.J., Brethouwer, G., Nieuwstadt, F.T.M.: A numerical investigation on the effect of the inflow conditions on the self-similar region of a round jet. Phys. Fluids **10**, 899–909 (1998)
5. Bogey, C., Bailly, C.: Large eddy simulations of transitional round jets: influence of the reynolds number on flow development and energy dissipation. Phys. Fluids **18**, 1–14 (2006)
6. Bradshaw, P.: The effect of initial conditions on the development of a free shear layer. J. Fluid Mech. **26**, 225–236 (1966)
7. Bradshaw, P., Ferriss, D.H., Johnson, R.F.: Turbulence in the noise-producing region of a circular jet. J. Fluid Mech. **19**, 591–624 (1963)
8. Crow, S.C., Champagne, F.H.: Orderly structure in jet turbulence. J. Fluid Mech. **48**, 547–591 (1971)
9. Deo, R.C., Mi, J., Nathan, G.J.: The influence of reynolds number on a plane jet. Phys. Fluids **20**, 075108 (2008). doi:10.1063/1.2959171
10. Freund, J.B.: Noise sources in low-reynolds-number turbulent jet at mach 0·9. J. Fluid Mech. **438**, 277–305 (2001)
11. Hussain, A.K.M.F.: Coherent structures—reality and myth. Phys. Fluids **26**, 2816–2850 (1983)
12. Hussein, H.J., Capp, S.P., George, W.K.: Velocity measurements in a high-reynolds-number, momentum-conserving, axisymmetric, turbulent jet. J. Fluid Mech. **258**, 31–75 (1994)
13. Ko, C.L., McLaughlin, D.K., Troutt, T.R.: Supersonic hot-wire fluctuation data analysis with a conduction end-loss correction. J. Phys. E: Sci. Instrum. **11**, 488–494 (1978)
14. Laufer, J., Kaplan, R.E., Chu, W.T.: Acoustic modeling of the jet noise abatement problem. In: Proc. Interagency Symp. on University Research in Transportation Noise, Stanford, 28–30 March 1973
15. Laufer, J., Yen, T.: Noise generation by a low-mach-number jet. J. Fluid Mech. **134**, 1–31 (1983)

16. Lush, P.A.: Measurement of subsonic jet noise and comparison with theory. J. Fluid Mech. **46**, 477–500 (1971)
17. McLaughlin, D.K., Morrison, D.K., Troutt, T.R.: Experiments on the instability waves in a supersonic jet and their acoustic radiation. J. Fluid Mech. **69**, 73–95 (1975)
18. Michalke, A.: On spatially growing disturbances in an inviscid shear layer. J. Fluid Mech. **23**, 521–544 (1965)
19. Michalke, A.: Survey on jet instability theory. Prog. Aerosp. Sci. **21**, 159–199 (1984)
20. Mollo-Christensen, E., Kolpin, M.A., Martucelli, J.R.: Experiments on jet flows and jet noise far-field spectra and directivity patterns. J. Fluid Mech. **18**, 285–301 (1964)
21. Moore, P.D., Slot, H.J., Boersma, B.J.: Simulation and measurement of flow generated noise. J. Comput. Phys. **224**, 449–463 (2007)
22. Morkovin, M.V.: Fluctuations and hot-wire anemometry in compressible flows. AGARDograph **24** (1956)
23. Oneill, P.L., Nicolaides, D., Honnery, D., Soria, J.: Autocorrelation functions and the determination of integral length with reference to experimental and numerical data. Fluid Mechanics Conference, Sydney, 13–17 December 2004
24. Panchapakesan, N.R., Lumley, J.L.: Turbulence measurements in axisymmetric jets of air and helium. Part 1. Air jet. J. Fluid Mech. **246**, 197–223 (1993)
25. Panda, J., Seasholtz, R.G.: Experimental investigation of the density fluctuations in high-speed jets and correlation with generated noise. J. Fluid Mech. **450**, 97–130 (2002)
26. Perry, A.E.: Hot-Wire Anemometry. Oxford University Press, Oxford (1982)
27. Quadrio, M., Luchini, P.: Integral space-time scales in turbulent wall flows. Phys. Fluids, **15**, 2219–2227 (2003)
28. Schram, C., Taubitz, S., Anthoine, J., Hirschberg, A.: Theoretica/emperical prediction and measurement of the sound produced by vortex pairing in a low mach number jet. J. Sound Vib. **281**, 171–187 (2005)
29. Stromberg, J.L., McLaughlin, D.K., Troutt, T.R.: Flow field and acoustic properties of a mach number 0.9 jet at a low reynolds number. J. Sound Vib. **72**, 159–176 (1980)
30. Swamy, N.V.C., Gowda, B.H.L., Lakshminath, V.R.: Auto-correlation measurments and integral time scales in three-dimensional turbulent boundary layers. Flow Turbul. Combust. **35**, 237–249 (1979)
31. Tam, C.K.W., Burton, D.E.: Sound generated by instability waves of supersonic flows. Part 2. Axisymmetric jets. J. Fluid Mech. **138**, 273–295 (1984)
32. Tam, C.K.W., Golebiowski, M., Seiner, M.: On the two components of turbulent mixing noise from supersonic jets. AIAA Pap. **96** (1996)
33. Tam, C.K.W., Morris, P.J.: The radiation of sound by the instability waves of a compressible plane turbulent shear layer. J. Fluid Mech. **98**, 349–381 (1980)
34. Tanna, H.K.: An experimental study of jet noise, part 1: turbulent mixing noise. J. Sound Vib. **50**, 405–428 (1977)
35. Troutt, T.R., McLaughlin, D.K.: Experiments on the flow and acoustic properties of a moderate-reynolds-number supersonic jet. J. Fluid Mech. **116**, 123–156 (1982)
36. VanderHeggeZijnen, B.G.: Measurements of the velocity distribution in a plane turbulent jet of air. Appl. Sci. Res. **7**, 256–276 (1958)
37. Viswanathan, K.: Aeroacoustics of hot jets. J. Fluid Mech. **516**, 39–82 (2004)
38. Wygnanski, I., Fiedler, H.: Some measurements in the self-preserving jet. J. Fluid Mech. **38**, 577–612 (1969)
39. Zaman, K.B.M.Q.: Effect of initial condition on subsonic jet noise. AIAA J. **23**(9), 1370–1373 (1985)
40. Zaman, K.B.M.Q.: Flow field and near and far sound field of a subsonic jet. J. Sound Vib. **106**, 1–16 (1986)